nature energy

SUPPLEMENTARY INFORMATION

https://doi.org/10.1038/s41560-017-0043-6

In the format provided by the authors and unedited.

Enabling the high capacity of lithium-rich anti-fluorite lithium iron oxide by simultaneous anionic and cationic redox

Chun Zhan[1], Zhenpeng Yao[2], Jun Lu[1]*, Lu Ma[3], Victor A. Maroni[1], Liang Li[4], Eungje Lee[1], Esen E. Alp[3], Tianpin Wu[3], Jianguo Wen[4], Yang Ren[3], Christopher Johnson[1], Michael M. Thackeray[1], Maria K. Y. Chan[4], Chris Wolverton[2]* and Khalil Amine[1]*

[1]Chemical Sciences and Engineering Division, Argonne National Laboratory, Argonne, IL, USA. [2]Material Science and Engineering Department, Northwestern University, Evanston, IL, USA. [3]X-ray Science Division, Argonne National Laboratory, Argonne, IL, USA. [4]Centre for Nanoscale Materials, Argonne National Laboratory, Argonne, IL, USA. Chun Zhan and Zhenpeng Yao contributed equally to this work. *e-mail: junlu@anl.gov; c-wolverton@northwestern.edu; amine@anl.gov

Supplementary Figures

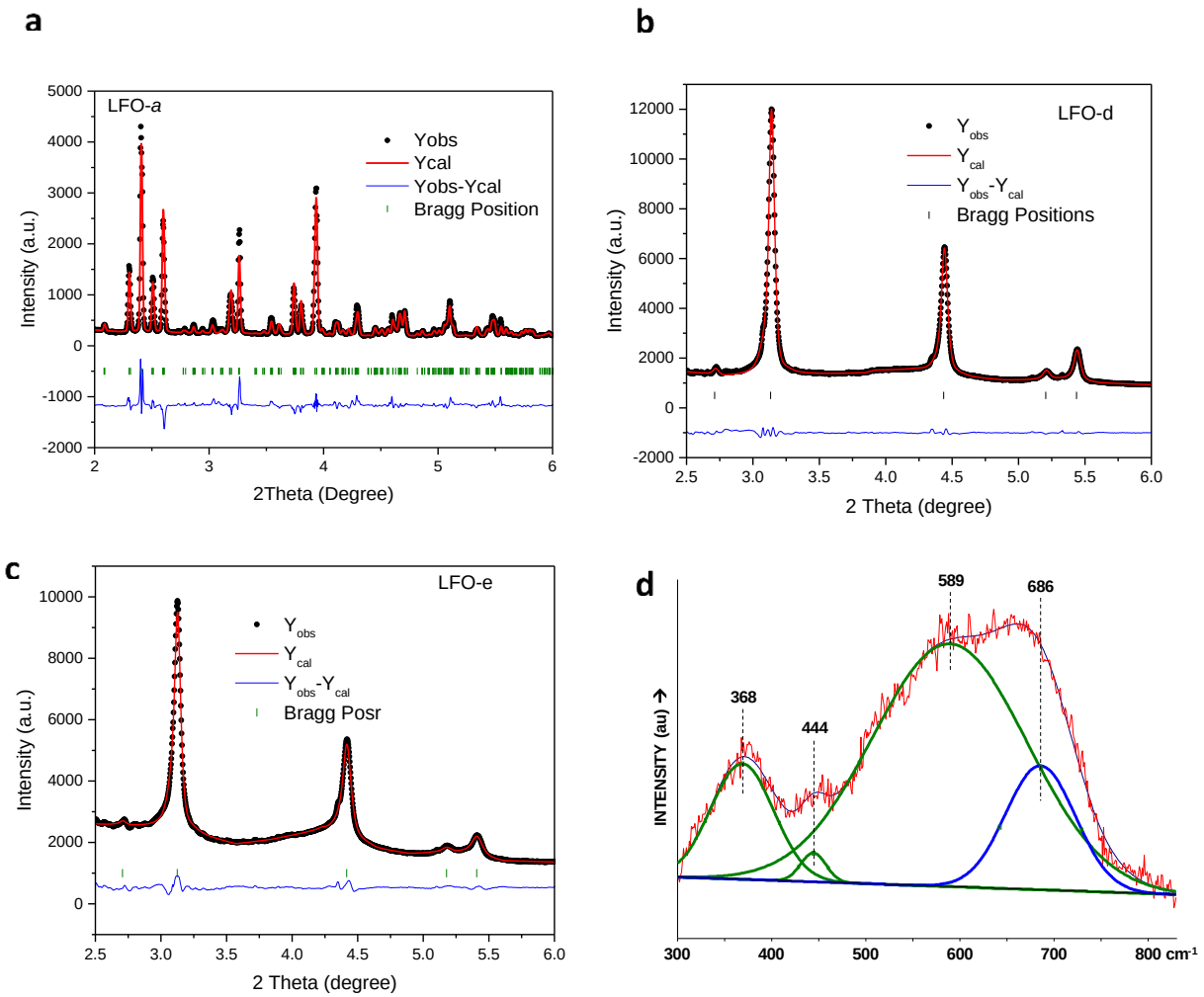

Supplementary Figure 1 | Refinement of XRD patterns and fitting of the Raman spectra. Panels **a** to **c** show the XRD refinements of LFO at point *i*, *iv*, and *v* in Fig. 1**b**. The XRD refinement parameters are listed in Supplementary Table 1. Panel **d** shows the fitting of Raman spectra of LFO at point *iii* in Fig. 1b. The bands at 686, 589, 444, 368 cm^{-1} can be associated with the metal oxygen vibrations of the FeO_6 octahedral, similar to a disordered cubic phase α-$LiFeO_2$.[1]

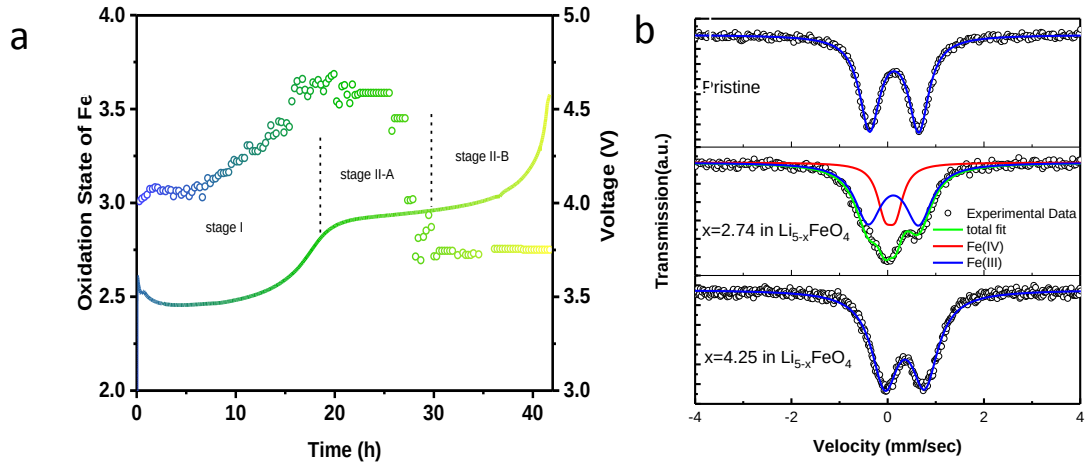

Supplementary Figure 2 | Additional analysis of the oxidation state of Fe in the first charging to 4.7V. **a,** Quantitative analysis by linear combination fitting of in-situ Fe K-edge XANES spectra in Fig. 4a. **b,** Ex-situ Mössbauer spectra of Li_5FeO_4 in the first charging to 4.7V. The corresponding Mössbauer parameters are listed in Supplementary Table 2.

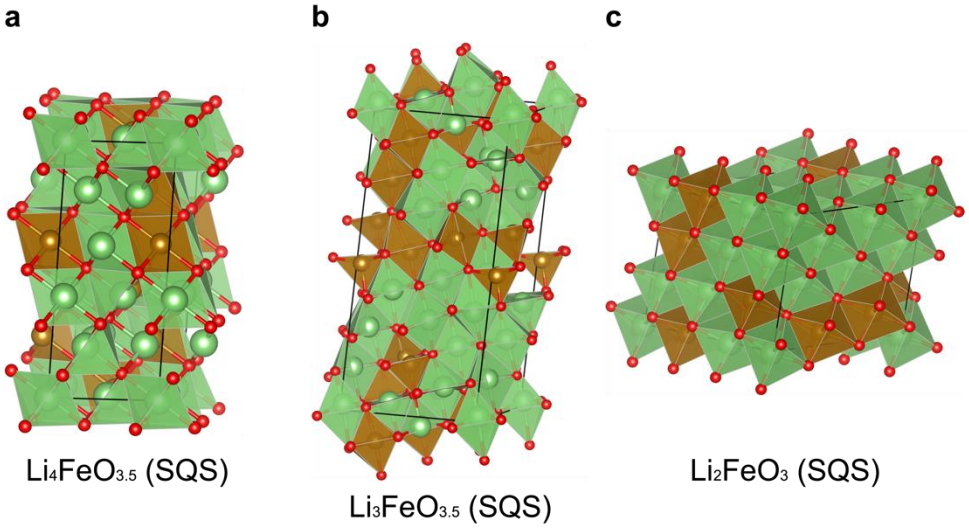

Supplementary Figure 3 | The disordered structures generated by the SQS method: (a) $Li_4FeO_{3.5}$, (b) $Li_3FeO_{3.5}$, and (c) Li_2FeO_3. Brown = Fe, green = Li, and red = O.

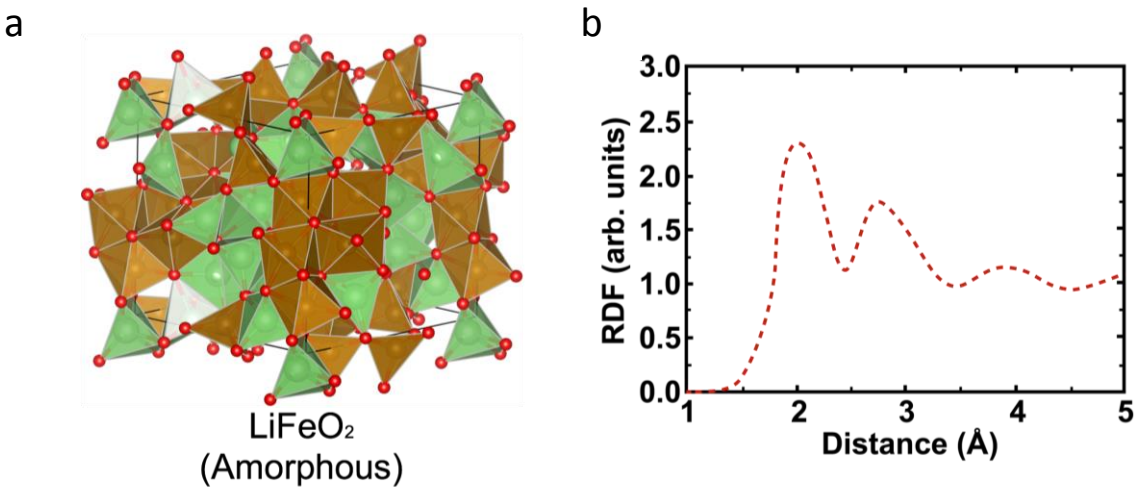

Supplementary Figure 4 | Calculated structure of $LiFeO_2$: (a) Generated amorphous structure of $LiFeO_2$ and (b) radial distribution function of amorphous $LiFeO_2$.

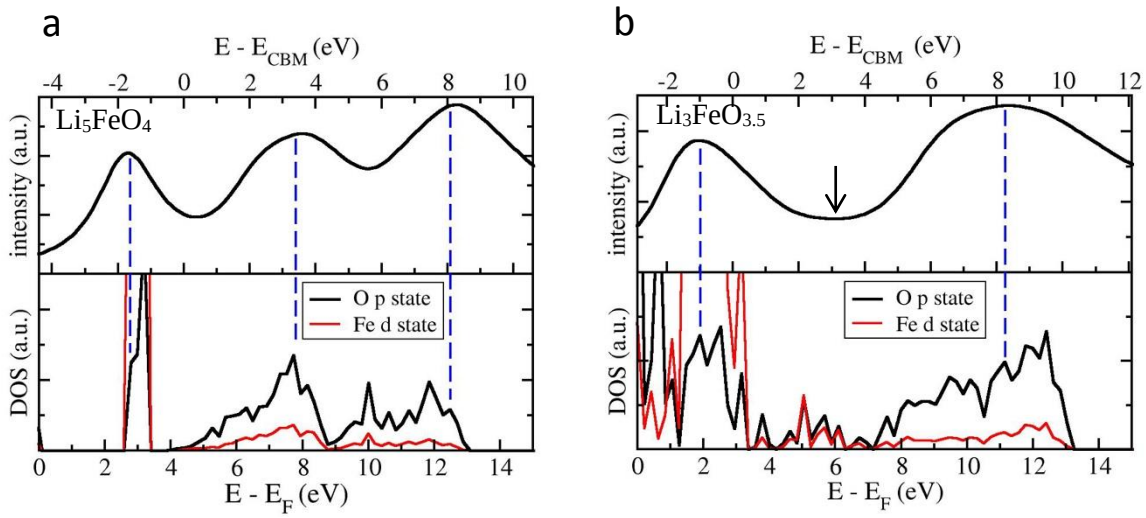

Supplementary Figure 5 | Simulated core-level spectrum and ground-state density of states (DOS) for (a) Li_5FeO_4 and (b) $Li_3FeO_{3.5}$. Upper panels show the simulated O K-edge spectra, and lower panels show the GGA-PBE DOS for O *p* states (black line) and Fe *d* states (red line). Zero energies in the lower and upper panels correspond to the Fermi level and conduction band minimum (CBM), respectively. The first peaks in the simulated spectra are below zero due to the excitonic effects. Blue dashed lines indicate the coincidence of the peaks.

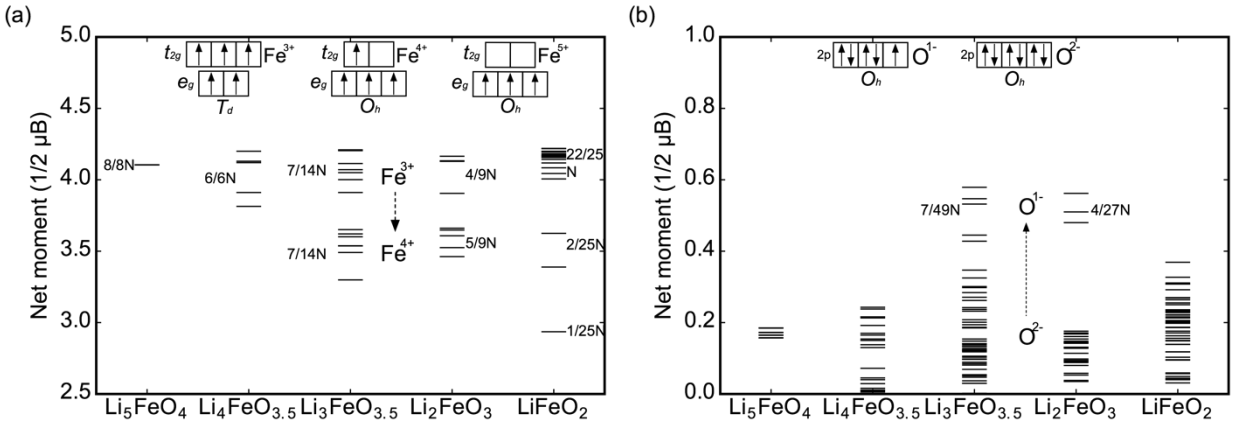

Supplementary Figure 6 | The magnetizations of (a) Fe ions and (b) oxygen ions in Li_5FeO_4, $Li_4FeO_{3.5}$, $Li_3FeO_{3.5}$, Li_2FeO_3, and $LiFeO_2$. The electronic configurations of Fe^{3+}, Fe^{4+}, Fe^{5+}, O^{1-}, and O^{2-} are presented.

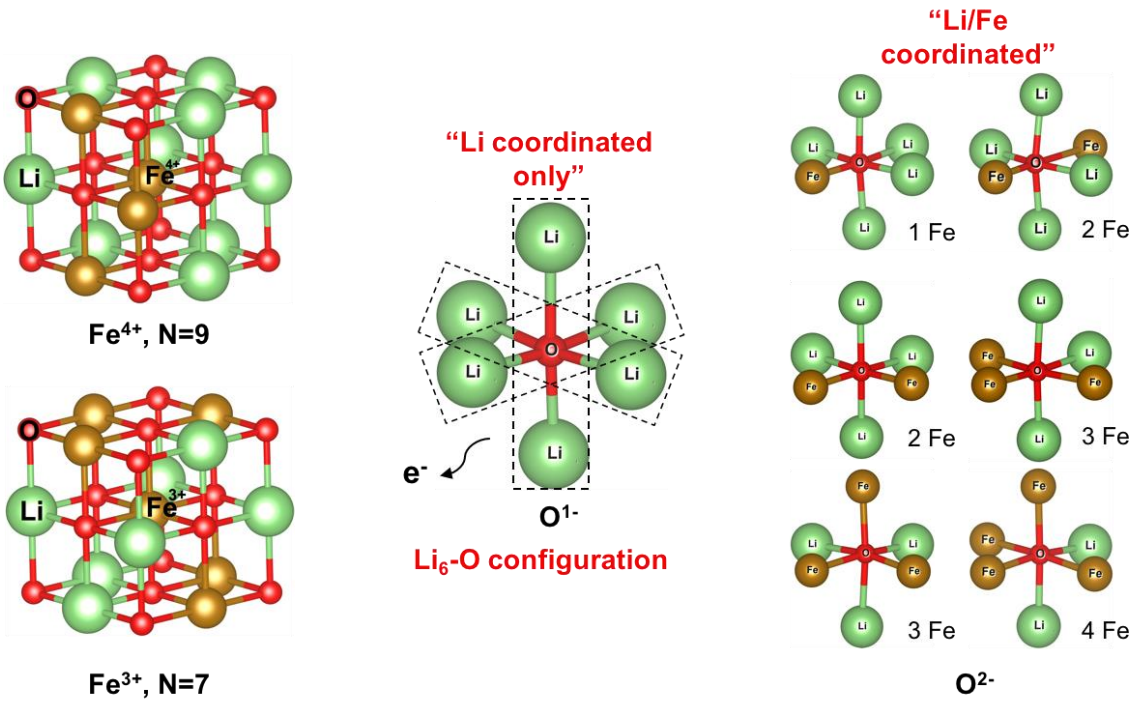

Supplementary Figure 7 | Local atomic environments for Fe and O ions in delithiated phases $Li_4FeO_{3.5}$, $Li_3FeO_{3.5}$, and Li_2FeO_3.

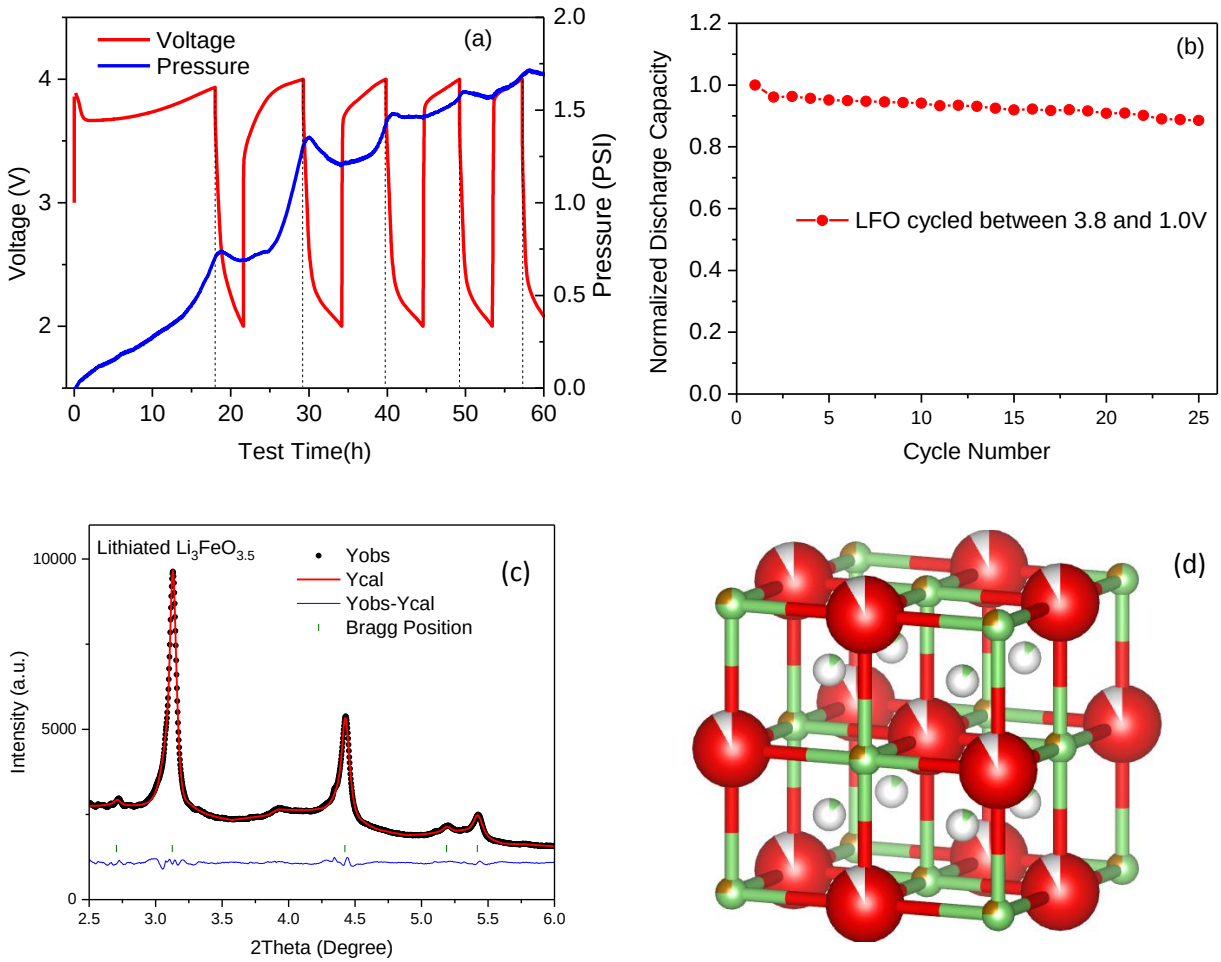

Supplementary Figure 8 | Additional characterization of the 3.8-1V cycling. ***a***, In-situ pressure measurement with cutoff voltage at 4.0 V. The voltage profile (red line) and the in-situ pressure (blue line) of the Li_5FeO_4/Li cells collected during cycles with upper cutoff voltage at 4.7 V. ***b***, Cycle performance of Li_5FeO_4/Li cell cycled between 3.8V and 1.0V. ***c,*** Ex-situ High Energy XRD pattern of the lithiated $L_3FeO_{3.5}$ collected at the end of the first discharging between 3.8 and 1V. The refinement was carried out using the disordered rocksalt crystal structure. The lattice parameters are a=b=c=4.085, α=β=γ=90º. The structure maintains but the lattice volume is enlarged after the lithiation, which may indicate the insertion of Li ions partially to the tetrahedral sites as shown in ***d***, Possible crystal structure of lithiated $Li_3FeO_{3.5}$ or noted as $Li_4FeO_{3.5}$.

Supplementary Tables

Supplementary Table 1 Summary of XRD Refinement Results in Supplementary Fig. 1.

Li_5FeO_4 pristine
Space group name P b c a
Lattice parameters: a= 9.225, b= 9.215, c=9.155 α=β=γ=90°
Structure parameters:

Atom	*x*	*y*	*z*	*occupancy*
Fe1	0.11855(39)	0.14570(24)	0.11682(35)	1
O1	-0.22840(75)	0.00935(181)	0.98081(97)	1
O2	0.25072(200)	0.25199(141)	0.22604(102)	1
O3	0.24468(109)	0.01978(127)	0.02321(103)	1
O4	0.02509(133)	0.00449(156)	0.24243(92)	1
Li1	0.88740(0)	0.35776(0)	0.11776(0)	1
Li2	0.37768(0)	0.12474(0)	0.16759(0)	1
Li3	0.14057(0)	0.86467(0)	0.11078(0)	1
Li4	0.09990(0)	0.11046(0)	0.83859(0)	1
Li5	0.32802(0)	0.87115(0)	0.88873(0)	1

LFO at point *iv* (after removal of about 2 Li ions)
Composition: $Li_3FeO_{3.6}$
Space group name F m -3 m
Lattice parameters: a=b=c= 4.068 α=β=γ=90°
Structure parameters:

Name	*x*	*y*	*z*	*occ.*
Li	0.00000(0)	0.00000(0)	0.00000(0)	0.750(0)
Fe	0.00000(0)	0.00000(0)	0.00000(0)	0.250(0)
O	0.50000(0)	0.50000(0)	0.50000(0)	0.902(0)*

LFO at point *v* (after removal of about 3 Li ions)
Composition: $Li_{2.1}Fe_{0.9}O_3$
Space group name: F m -3 m
Lattice parameters: a=b=c= 4.104 α=β=γ=90°
Structure parameters:

Name	*x*	*y*	*z*	*occ.*
Li	0.00000(0)	0.00000(0)	0.00000(0)	0.698(1)
Fe	0.00000(0)	0.00000(0)	0.00000(0)	0.302(1)
O	0.50000(0)	0.50000(0)	0.50000(0)	1.000(0)

Note:

* The oxygen vacancy calculated from XRD refinement is about 10%, which is close to the amount calculated from DFT simulation (12.5%).

Supplementary Table 2. Mössbauer parameters for samples in Supplementary Figure 2b

x in $Li_{5-x}FeO_4$	Fe species	% Area	Isomer Shift (mm/s)	Quadrupole Splitting (mm/s)
0	Fe(III)	100	0.14	1.02
2.74	Fe(III)	70	0.12	1.04
	Fe(IV)	30	0.055	0.22
4.25	Fe(III)	100	0.36	0.82

Supplementary Notes

Density Functional Theory (DFT) Calculations

Methodology

Since the delithiated phases of $Li_4FeO_{3.5}$, $Li_3FeO_{3.5}$, and Li_2FeO_3 adopt disordered cubic structures, the corresponding computational unit cells were built (Supplementary Fig. 3) using the special quasi-random structure (SQS) method. Starting from the cubic rock-salt cell, supercells containing 30 cation sites/30 anion sites, 56 cation sites/56 anion sites, and 27 cation sites/27 anion sites were created for $Li_4FeO_{3.5}$, $Li_3FeO_{3.5}$, and Li_2FeO_3, respectively. We populated the cation sites randomly with Fe and Li in ratios of 4:1, 3:1, and 2:1 for $Li_4FeO_{3.5}$, $Li_3FeO_{3.5}$, and Li_2FeO_3, respectively. Vacancies were introduced to the anion sites of the $Li_4FeO_{3.5}$ and $Li_3FeO_{3.5}$ structures randomly in ratios of 3:7 and 1:7 with respect to O while all the anion sites of Li_2FeO_3 were occupied by O. All SQSs were generated based on a Monte Carlo algorithm implemented in ATAT[2-12] with the constraint that the pair and triplet correlation functions of the SQS are identical to those of the statistically random Li/Fe population of cation sites and O/vacancy population of anion sites at least up to the third nearest neighbor. According to the XRD observations mentioned in the main text, the $LiFeO_2$ phase shows features of amorphorization. A corresponding amorphous computational cell containing 100 atoms was constructed (Supplementary Fig. 4) by *ab initio* molecular dynamics (AIMD) simulation to a liquid-like state at 2900 K, followed by a rapid temperature quench and energy minimization.[13,14] The liquid state configurations were equilibrated over two picoseconds under a constant-volume, constant-temperature canonical (NVT) ensemble. The quench was enabled through an AIMD run starting at the equilibration temperature

and dropping down to 300 K at the rate of 1 K/fs, followed by conjugate-gradient relaxation of atomic coordinates and cell parameters, until the force on each atom fell below 10^{-2} eV/Å.

The oxygen K-edge spectra simulations were performed using the OCEAN package[15,16] that implements the Bethe-Salpeter equation (BSE) approximation, which is built upon the DFT ground-state charge density and Kohn-Sham Hamiltonian. The DFT routine was performed with the ABINIT package.[17] Local density approximation (LDA) was employed for the exchange-correlation functional. Norm-conserving pseudopotentials from the ABINIT distribution were used, in conjunction with a cutoff energy of 70 Ry. The size of k-point grid used to solve the Kohn-Sham states for BSE was 4×4×4 for Li_5FeO_4 and 3×3×2 for $Li_3FeO_{3.5}$, and the screening calculations for both structures used a 2×2×2 k-point grid. The number of unoccupied bands used for the BSE calculation is at least 800, and the screened core-hole potential calculation includes at least 1300 bands. Each oxygen atom in the simulation cell was considered as the absorbing atom. The polarization vectors were set to be [100], [010], and [001], and the final spectrum was obtained by averaging the spectra generated by all oxygen atoms using each of the polarization vectors.

O Core-Level Spectra

Previous studies have demonstrated that the O 1*s* core hole is relatively well screened by other valence electrons, and the excitonic effects would influence only the intensity distribution of unoccupied states, without introducing additional excitonic excitations.[18,19] Therefore, the absorption peaks in the O K-edge spectra can reasonably be attributed to the peaks in the ground-state density of the oxygen p states.[19,20]

Supplementary Figure 5a compares the simulated O K-edge spectrum of Li_5FeO_4 with its ground-state DOS. It can be inferred from the DOS plot that the unoccupied states consist of three sub-bands, whose positions roughly coincide with the three peaks in the simulated spectra. The

lowest-energy sub-band appears to be the narrowest, which is also consistent with the simulated spectrum. The DOS plot clearly shows Fe-*d* and O-*p* hybridization. The hybridized state at 2.5–3.5 eV is dominated by Fe-*d* characteristic, while the higher-energy sub-bands have more O-*p* than Fe-*d* character, but also have additional Fe-*s* and Li components and are highly delocalized. Similarly, plotted in Supplementary Fig. 5b are the simulated $Li_3FeO_{3.5}$ O K-edge spectrum and the ground-state DOS. The low-energy region of the DOS plot is again dominated by the Fe contribution, and the delocalized O-*p* and Fe-*d* hybridized states seemingly manifest themselves as the broad peak in the simulated spectrum that is higher in energy (7.1–13.2 eV). However, unlike that of Li_5FeO_4, for $Li_3FeO_{3.5}$, the Fe and O contributions in the 3.5–7.1 eV region are small, which is likely to result in the valley seen in the simulated spectrum (as indicated by the arrow). Therefore, the distinct features (number of peaks, peak splitting, etc.) of Li_5FeO_4 and $Li_3FeO_{3.5}$ core-level spectra can qualitatively be explained by using the ground-state DOS. It is informative to show the DOS taking into account core-hole effects or to further decompose the DOS for bonding interaction analysis, but such studies are beyond the scope of this work.

Magnetizations and valence states of Fe and O ions

We determined the oxidation states of Fe and oxygen ions in the original Li_5FeO_4 and the following delithiated phases ($Li_{5-x}FeO_{4-y}$): $Li_3FeO_{3.5}$, Li_2FeO_3 and $LiFeO_2$. The oxidation states were determined by comparing calculated magnetizations of Fe and O ions with the number of unpaired electrons of the corresponding ions with known oxidation states. The numbers of unpaired electrons for Fe^{3+} (tetrahedrally coordinated), Fe^{4+} (octahedrally coordinated), and Fe^{5+} (octahedrally coordinated) are 5, 4, and 3, respectively, as shown in Supplementary Fig. 6a. In the original Li_5FeO_4 phase, the magnetizations are around 4.1 for all Fe ions, implying an overall 3+ oxidation state. After 2 Li ions and a slight amount of O were extracted ($x = 2$, $y = 0.5$), seven Fe

ions show magnetizations around 3.5, while the other seven remain around 4.1, indicating that half of the Fe ions have been oxidized to 4+. After lithiating the $Li_3FeO_{3.5}$ back to $Li_4FeO_{3.5}$ (x = 1, y = 0.5) during the reversible cycling between 1 V and 3.8 V, all Fe ions exhibit magnetizations around 4.0, indicating a complete reduction of Fe^{4+} to Fe^{3+}. After the extraction of 3 Li and 1 O per formula unit (x = 3, y = 1), the Fe magnetization distribution stays almost the same as the $Li_3FeO_{3.5}$ phase; whereas, four Fe ions show magnetizations around 4.1, corresponding to the oxidation state of 3+, and five Fe ions show magnetizations around 3.5, corresponding to the oxidation state of 4+. In the final phase (x = 4, y = 2), most Fe ions (22 of 25) show magnetizations around 4.1, corresponding to oxidation state of 3+ and indicating the reduction of most Fe^{4+} by additional O removal. Three Fe ions show smaller magnetizations around 3.5 and 3, corresponding to oxidation states of 4+ and 5+, which are expected considering the complex local environments for specific Fe ions in the amorphous structure.

A similar analysis was performed for the magnetization of the oxygen ions. The magnetizations of oxygen ions in the original Li_5FeO_4 are close to 0, corresponding to an overall valence state of 2- for oxygen ions. After the extraction of 2 Li and 0.5 O per formula unit (x = 2, y = 0.5), several oxygen ions (7 of 49) show increased magnetizations around 0.5 (Supplementary Fig. 6b), indicating the partial oxidation of O^{2-} to O^{1-}. In the following re-lithiated phase ($Li_4FeO_{3.5}$), all the oxygen ions exhibit magnetizations around 0 again, indicating the full reduction of O^{1-} to O^{2-}. With further Li and O removal (x = 3, y = 1), a similar portion of oxygen ions (4 of 27) show increased magnetizations. In the final phase (x = 4, y = 2), magnetizations of oxygen ions show a relatively wide distribution corresponding to various oxygen-ion local environments in the amorphous structure. No oxygen ions show magnetization above ~0.4, indicating the overall oxidation state of 2- for oxygen ions.

Effect of local atomic environments on the electronic states of O and Fe ions

The atomic environments of Fe and O ions in cation-disordered rocksalt phases $Li_4FeO_{3.5}$, $Li_3FeO_{3.5}$, and Li_2FeO_3, and their effects on the electronic states of O ions, were examined and are shown in Fig. 5 and Supplementary Fig. 7. During the first delithiation step of Li_5FeO_4 with 2 Li ion and slight (0.5) O removal, a concurrent phase transition occurs from antifluorite to cation-disordered pseudo-cubic, which brings Li-excess O ion configurations (Fig. 5d) to the system. In the resulting $Li_3FeO_{3.5}$ phase, all the O^{1-} ions are identified to be in the particular "Li_6-O" configuration (Fig. 5d) with only Li ion coordination (first nearest neighbors), while the remaining oxygen ions stay as O^{2-} with at least one Fe first nearest neighbor. The projected DOS (pDOS) of the oxygen *2p* states and iron *3d* states of these two configurations are shown in Figs. 5b-c. For the Li_6-O configuration (Fig. 5b), the contribution from oxygen to the valence band immediately below the Fermi level is significantly larger than that from Fe, which shows that electrons can be readily extracted from oxygen when the system is being oxidized. On the contrary, for the partially Fe-coordinated configurations (Fig. 5c), the Fe-O bonds show strong covalency, and both cationic and anionic activities can be expected during further charging. The cationic/ionic redox that occurs during delithiation can qualitatively be demonstrated *via* the locations of the holes generated by extracting electrons from $Li_3FeO_{3.5}$. The isosurface shown in the inset of Fig. 5b is constructed by visualizing the charge density in the energy range between 0 and −1 eV, which roughly corresponds to the removal of one electron. Apparently, the hole is localized around the oxygen atom in the center of Li_6-O, which signals the ionic redox behavior. Previous study has shown the elongated charge density isosurface around the oxygen ion in a linear Li-O-Li bond,[21] whereas the shape of the isosurface in the Li_6-O configuration is nearly spherical, which is due to the isotropic bonding of the six surrounding Li atoms. This result indicates that on further delithiation, the O^{1-}

in the local Li-excess environment originating from this particular Li_6–O configuration can give out one labile electron and become O^0, consistent with a previous study.[21] The irreversible delithiation from $Li_3FeO_{3.5}$ to Li_2FeO_3 and $LiFeO_2$ proceeds by gradual oxidation of O^{1-} to O^0 and elimination of these specific Li_6-O configurations (Fig. 5d). Nevertheless, these Li_6-O configurations would be retained during the re-lithiation to $Li_4FeO_{3.5}$, with the oxygen ions being reduced to O^{2-}. As shown in Fig. 5a, the Fe contribution to the states lying below the Fermi level is almost negligible compared with that from oxygen, and the isosurface corresponding to one electron removal is also centered around the oxygen ion; therefore, significant anionic redox can be expected. Labile electrons extracted from the Li_6-O configuration will enable the partial oxidation of O^{2-} to O^{1-}. The O^{2-}/O^{1-} redox couple in this specific configuration, along with the Fe^{3+}/Fe^{4+} redox couple, thus plays a key role during the reversible cycling between $Li_4FeO_{3.5}$ and $Li_3FeO_{3.5}$.

Supplementary References:

1 Barik, R., Leung, K. T. & Mohapatra, M. Solvent specific synthesis of nano corpse flowery lithiated iron oxide as an energy storage and gas sensing material. *New J. Chem.* **40**, 475-484 (2016).

2 Cockayne, E. & van de Walle, A. Building effective models from scarce but accurate data: Application to an alloy cluster expansion model. *Phys. Rev. B* **81,** 12104–12113 (2010).

3 van de Walle, A. Multicomponent multisublattice alloys, nonconfigurational entropy and other additions to the Alloy Theoretic Automated Toolkit. *Calphad* **33,** 266–290 (2009).

4 van de Walle, A. Methods for first-principles alloy thermodynamics. *JOM - J. Min. Met. Mat. S.* **65,** 1523–1532 (2013).

5 van de Walle, A. A complete representation of structure-property relationships in crystals. *Nat. Mater.* **7,** 455–458 (2008).

6 van de Walle, A. & Asta, M. Self-driven lattice-model Monte Carlo simulations of alloy thermodynamic properties and phase diagrams. *Model. Simul. Mater. Sc.* **10,** 521–539 (2002).

7 van de Walle, A., Asta, M. & Ceder, G. The Alloy Theoretic Automated Toolkit: A user guide. *Calphad* **26,** 539–553 (2002).

8 van de Walle, A. & Ceder, G. Automating first-principles phase diagram calculations. *J. Phase Equilib.* **23,** 348–368 (2002).

9 van de Walle, A. & Ellis, D. First-principles thermodynamics of coherent interfaces in samarium-doped ceria nanoscale superlattices. *Phys. Rev. Lett.* **98,** 266101–266118 (2007).

10 van de Walle, A. *et al.* Ab initio calculation of anisotropic interfacial excess free energies. *Phys. Rev. B* **89,** 184101–184111 (2014).

11 van de Walle, A., Hong, Q., Kadkhodaei, S. & Sun, R. The free energy of mechanically unstable phases. *Nat. Commun.* **6,** 7559–7564 (2015).

12 van de Walle, A. *et al.* Efficient stochastic generation of special quasirandom structures. *Calphad* **42,** 13–18 (2013).

13 Bin, H. *et al.* A high-performance anode material based on $FeMnO_3$/graphene composite. *J. Alloys Compd.* **695,** 1223–1230 (2017).

14 Li, Q. *et al*. Electrochemistry of Selenium with Sodium and Lithium: Kinetics and Reaction Mechanism. *ACS Nano* **10,** 8788–8795 (2016).

15 Vinson, J., Rehr, J. J., Kas, J. J. & Shirley, E. L. Bethe-Salpeter equation calculations of core excitation spectra. *Phys. Rev. B* **83**, 115106 (2011).

16 Gilmore, K. *et al.* Efficient implementation of core-excitation Bethe-Salpeter equation calculations. *Comput. Phys. Commun.* **197**, 109–117 (2015).

17 Gonze, X. *et al.* First-principles computation of material properties: the ABINIT software project. *Comput. Mater. Sci.* **25**, 478–492 (2002).

18 Qiao, R., Chuang, Y., Yan, S. & Yang, W. Soft X-ray irradiation effects of Li_2O_2, Li_2CO_3 and Li_2O revealed by absorption spectroscopy. *PLoS One* 7, e49182 (2012).

19 Jiang, N. & Spence, J. C. H. Core-hole effects on electron energy-loss spectroscopy of Li_2O. *Phys. Rev. B* **69**, 115112 (2004).

20 Pchelkina, Z. V. *et al.* Electronic structure of Li_2RuO_3 studied by LDA and LDA+DMFT calculations and soft x-ray spectroscop. *Phys. Rev. B* **91**, 115138 (2015).

21 Seo, D. *et al.* The structural and chemical origin of the oxygen redox activity in layered and cation-disordered Li-excess cathode materials. *Nat. Chem.* **8**, 692-697 (2016).